Focusing cold neutrons with multiple biconcave lenses for small-angle neutron scattering

S.-M. Choi[ab*], J. G. Barker[a], C. J. Glinka[a], Y. T. Cheng[c] and P. L. Gammel[d]

[a]*Center for Neutron Research, National Institute of Standards and Technology, Gaithersburg, MD 20899-8562 , USA*
[b]*Department of Materials and Nuclear Engineering, University of Maryland, College Park, MD 20742 , USA*
[c]*NeuTek, Darnestown, MD 20878, USA*
[d]*Bell Laboratories, Lucent Technologies, Murray Hill, NJ 07974, USA*
Email:sungmin.choi@nist.gov

The focusing of a cold neutron beam by multiple biconcave lenses has recently been proposed as a practical means of extending the lower limit of Q in conventional, long flight-path small-angle neutron scattering (SANS) instruments. To test the feasibility of this approach, we have carried out extensive measurements on one of the 30 m SANS instruments at NIST of the focusing characteristics of a set of 28 biconcave MgF_2 lenses. The focused beam profile has been measured over several orders of magnitude using high resolution neutron auto-radiography. The focusing lens configuration outperforms the pinhole collimation at Q_{min} lower than 0.004 Å^{-1}. At Q_{min} = 0.001 Å^{-1}, the intensity gain of the lens configuration over the pinhole collimation is greater than one order of magnitude.

Keywords: small-angle neutron scattering, neutron focusing, refractive lens.

1. Introduction

The focusing of a cold neutron beam by multiple biconcave lenses has recently been demonstrated (Eskildsen et al, 1998) and proposed as a practical means of improving the minimum Q of conventional SANS instruments which use circular apertures separated by distances of several meters (pinhole collimation) to collimate the incident beam. To investigate this proposal, we have measured in detail the shape of the focal spot produced by the same set of biconcave MgF_2 lenses used by Eskildsen et al (1998) and have compared the results with both Monte Carlo (MC) simulations of the beam profile and measurements of beam profiles made under optimal pinhole collimation conditions (Mildner & Carpenter, 1984).

Since refractive indices for cold neutrons (wavelength ~ 10 Å) differ from unity by at most a few parts in 10^5, grazing incidence reflection optics have long been considered as the most promising means for focusing neutrons for applications such as small-angle neutron scattering (SANS). Numerous attempts (Maier-Leibnitz & Springer, 1963, Barker & Glinka, 1993, Lartigue et al., 1995, Alefeld et al., 1997) over more than 30 years to produce reflective surfaces for neutrons have been vitiated, however, by SANS from the mirror surfaces themselves, which blurs the focus. The best mirrors produced thus far are only marginally better for SANS than pinhole collimation (Alefeld et al., 1997).

For most materials, the neutron refractive index, n, is less than unity. Therefore, in contrast to light where n is greater than unity, a concave lens is convergent while a convex lens is divergent. For a biconcave lens, the focal length, f_o, is given as (Sears, 1989),

$$f_o = \frac{R}{2(1-n)} = \frac{R}{\xi} = \left(\frac{R}{\rho b_c}\right)\left(\frac{\pi}{\lambda^2}\right) \qquad (1)$$

where R is the radius of curvature of the biconcave lens, $\xi = (\lambda^2 / \pi)\rho b_c$, ρ the atomic density, b_c the bound coherent scattering length of an atom, and λ the wavelength of incident neutrons. When N thin biconcave lenses are used in series, the focal length, f, is given as, $f = f_o/N$. Here, it should be noticed that the focal length of a lens depends on λ^{-2}, i.e. a lens is strongly chromatic. Therefore, neutrons with well-defined wavelength are required for good focusing. Most SANS instruments at steady state neutron sources utilize neutrons with a wavelength spread $\Delta\lambda/\lambda$ = 10 - 15 %. Therefore a certain amount of chromatic aberration is expected. According to Gaussian optics (Born & Wolf, 1975), the focal length obeys $1/f = 1/L_1 + 1/L_2$, where L_1 is the distance from source to the lenses and L_2 is the distance from the lenses to the focal point.

For a biconcave lens made of MgF_2 with R = 2.5 cm, ξ = 1.6 × 10^{-4} for 10 Å neutrons and f_o = 156 m. Therefore, for the 30 m SANS instrument at NIST, with $L_1 = L_2$ = 15 m, 21 MgF_2 lenses are needed to focus 10 Å neutrons.

2. SANS Collimation Geometry

Figure 1 a) shows a schematic diagram of the conventional pinhole collimation used in long flight-path SANS instruments. The source and sample apertures, and the distances L_1 and L_2 define the beam size at the detector position. For $L_1 = L_2$, the optimal pinhole condition is $A_{1P} = 2 A_{2P}$ (Mildner & Carpenter, 1984), and, therefore, the beam profile at the detector is approximately triangular with a base width, $B_P = 2 A_{1P}$. In this case, the minimum accessible scattering vector, Q, is

$$Q_{min} = k\theta_{min} = c_P k \frac{A_{1P}}{L_2} \qquad (2)$$

where $k = 2\pi / \lambda$, A_{1P} is the diameter of source aperture and c_P (=1 in ideal case) is a smearing factor which includes detector resolution, beam spreading due to gravity, and parasitic scattering. The beam intensity (n/sec) on sample I_P is given as,

$$I_P(n/\sec) = \frac{d^2\phi}{d\Omega d\lambda} \delta\lambda \left(\frac{A_{source}A_{sample}}{L_1^2}\right) \qquad (3)$$

where ϕ is the neutron flux, $A_{source} = A_{1P}^2/4$ and $A_{sample} = A_{2P}^2/4 = A_{1P}^2/16$. Using equation (2) and $L_1 = L_2$, equation (3) can be rewritten as

$$I_P = \frac{d^2\phi}{d\Omega d\lambda} \delta\lambda \left(\frac{\pi L_1}{8}\right)^2 \left(\frac{Q_{min}}{c_P k}\right)^4 . \qquad (4)$$

Figure 1 b) shows a schematic diagram of the focusing lens geometry. When $L_1 = L_2$, the size of a perfectly focused beam at the detector is same as the source size, $B_L = A_{1L}$. It should be noticed that the beam size at the detector is independent of the sample aperture size. Therefore, sample sizes up to the size of the lens opening can be
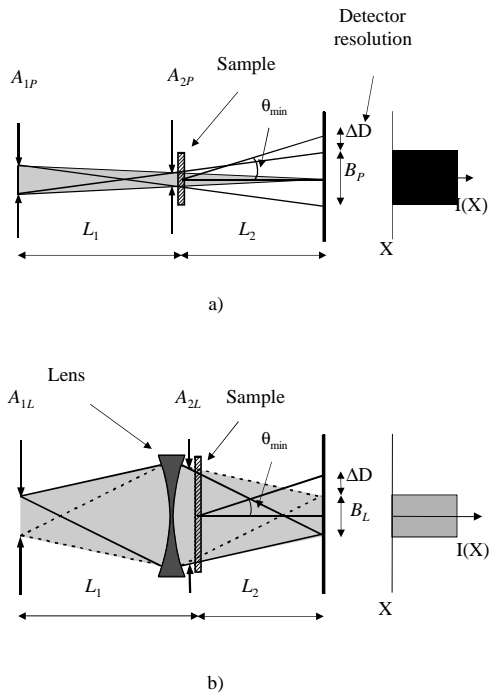
Figure 1
Beam collimation geometry for SANS. a) Pinhole collimation geometry, b) Focusing lens geometry.

used to increase intensity without affecting the beam size at the detector. In this lens configuration, the minimum Q is given as

$$Q_{\min} = c_L k \frac{A_{1L}/2}{L_2} \quad (5)$$

where c_L is a smearing factor which includes detector resolution, chromatic aberration, gravity effect, and any scattering by the lenses. It can easily be shown that the intensity on sample can be expressed as,

$$I_L = T_L \frac{d^2\phi}{d\Omega d\lambda} \delta\lambda \left(\frac{\pi A_{2L}}{2}\right)^2 \left(\frac{Q_{\min}}{c_L k}\right)^2 \quad (6)$$

where T_L is the neutron transmission of the lenses.

From equations (4) and (6), it should be noticed that I_L is proportional to $Q_{\min}^2$ while I_P is proportional to $Q_{\min}^4$. Therefore, as $Q_{\min}$ becomes smaller, the intensity on sample decreases in both cases, but much faster for pinhole collimation than for focusing lens collimation. Therefore, there is a crossover at a certain value of $Q_{\min}$ below which focusing outperforms pinhole collimation. For a given $Q_{\min}$, the gain provided by the lenses compared with pinhole collimation can be defined as the ratio of the intensities on the sample. From equations (4) and (5),

$$Gain = \frac{I_L}{I_P} = \left(\frac{A_{1L}}{A_{1P}}\right)^2 \left(\frac{A_{2L}}{A_{2P}}\right)^2 \left(\frac{c_P}{c_L}\right)^2 T_L . \quad (7)$$

In the ideal case where $c_P = c_L = 1$ and $T_L = 1$, the gain is simply a product of the squares of the ratios of aperture diameters. For example, when $L_1 = L_2$, to make a 2 cm diameter beam at the detector, in the lens configuration we can use $A_{1L} = 2$ cm and $A_{2L} = 1.5$ cm

while in the pinhole collimation we need to use $A_{1P} = 1$ cm and $A_{2P} = 0.5$ cm. Then the gain is $4 \times 9 = 36$. In practice, this ideal gain will be reduced by the intensity attenuation by the lenses and the smearing factors.

The focusing characteristics of a set of 28 biconcave MgF_2 lenses, including the effects of chromatic aberration due to the wavelength spread in the incident beam, and distortion due to gravity, have been extensively studied by MC simulations and measurements on one of the 30 m SANS instruments at NIST. Here we present a case where $\lambda = 8.15$Å, $\Delta\lambda/\lambda = 11\%$, $L_1 = 15.5$ m, $L_2 = 15.8$ m, $A_1 = 0.95$ cm and $A_2 = 1.59$ cm were used. The MC simulations of the beam intensity distributions at the detector position are presented in Figure 2 a) (without lenses) and Figure 2 b) (with 28 MgF_2 biconcave lenses that have a radius of curvature of 2.5 cm and a center thickness of 1 mm). In this simulation, a triangular wavelength distribution is assumed and the gravity effect is included. It can be clearly seen that the beam with the lenses is much smaller than one without the lenses and is more intense (8.5 times) at the center of the beam. The size of the focused beam should be same as the source aperture size, but here the beam is somewhat larger than the source aperture for two reasons. First, chromatic aberration due to the wavelength spread of the incident beam appears in both the horizontal and vertical directions. For neutrons with shorter (or longer) wavelengths than the mean wavelength, which satisfies the Gaussian optics relation, the detector position at L_2 is before (or after) the focal plane and the beam at L_2 is larger than the source aperture. Second, the beam is elongated along the vertical direction due to gravity. The short wavelength neutrons appear at the top and the longer wavelength neutrons at the bottom.

In order to measure the detailed shape of the focused beam intensity, a high resolution (≤ 0.05 mm), wide dynamic range (greater than 5 orders of magnitude), imaging technique was utilized: an image transfer technique based on neutron activation of dysprosium foil followed by off-line exposure of a gamma-ray-sensitive image plate. Therefore the beam intensity at the focal plane could be measured over 5 orders of magnitude, essentially free of any smearing due to finite detector resolution. Figure 2 c) shows a 2D image of the focused beam measured with the image transfer technique. In this measurement, all conditions were the same as those used in the MC simulation presented in Figure 2 b). The measured 2D distribution of the focused beam is qualitatively very close to the MC simulation.

To understand the properties of the focused beam in a more quantitative way, 1D profiles across the peak intensity region were obtained from the 2D images. Figure 3 shows the 1D profiles along the vertical direction. A high signal-to-noise ratio (ratio of the peak intensity to the base line intensity) is important for the focused beam to be useful for SANS experiments. To determine the signal-to-noise ratio and the detailed shape at the tail, the focused beam profiles were examined on log scale. The measured profile shows a signal-to-noise ratio greater than 10^4 which is very suitable for SANS experiments. The agreement between the measured and the simulated profiles is quite good down to the intensity level 10^{-3}, below which the measured profile shows a wider beam width than the simulated one. This deviation can be explained by three factors. First, the bump at $Y = 0$ mm position is due to fast neutrons coming from the reactor. Second, while in the simulation a perfect triangular wavelength distribution was assumed, the actual wavelength distribution has an additional tail beyond the cut off of a triangular distribution (Glinka et al., 1998) which contributes a further chromatic aberration and spreading due to
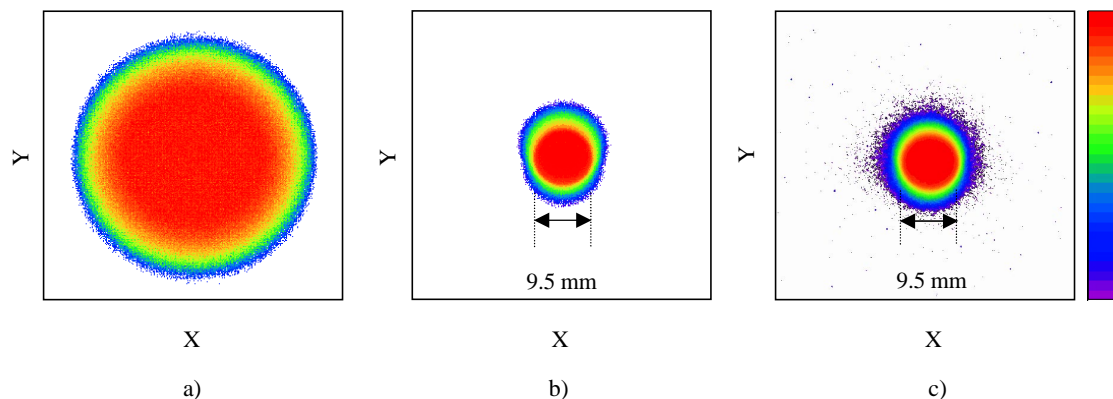
Figure 2
2D Images of focused and unfocused beams. $\lambda = 8.15$Å, $\Delta\lambda/\lambda = 11\%$, $L_1 = 15.5$ m, $L_2 = 15.8$ m, $A_1 = 0.95$ cm and $A_2 = 1.59$ cm. a) Unfocused beam: MC simulation. b) Focused beam with 28 MgF$_2$ biconcave lenses: MC simulation. c) Focused beam with 28 MgF$_2$ biconcave lenses: measured with image transfer technique. The size of boxes is 40 mm x 40 mm.

gravity. Third, the lenses produce small-angle scattering but, from a practical point of view, it is negligible. The width of the simulated beam at the 10^{-4} intensity level is 1.89 cm which is twice the size of the source aperture (0.95 cm). Of the total enlargement of 0.94 cm, 0.66 cm (determined from a horizontal profile that has no broadening due to gravity) is due to the chromatic aberration and 0.28 cm is due to gravity.
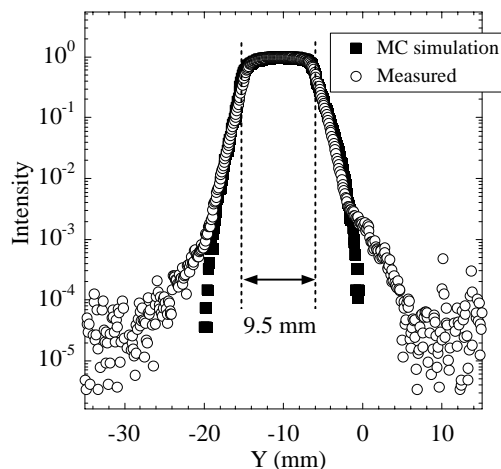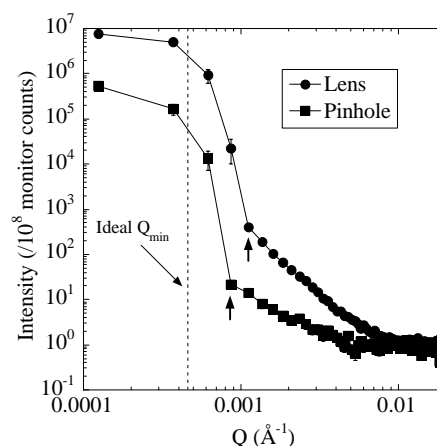

Figure 3
1D profiles of focused beam images in figure 2 along the vertical direction. $\lambda = 8.15$Å, $\Delta\lambda/\lambda = 11\%$, $L_1 = 15.5$ m, $L_2 = 15.8$ m, $A_{1L} = 0.95$ cm and $A_{2L} = 1.59$ cm. 28 MgF$_2$ biconcave lenses were used.

3. Intensity Gain of the Focusing Lens Collimation

We have measured the beam intensity profiles for the lens and pinhole configurations under conditions that produce the same ideal Q_{min}. From these we have determined the intensity gain as defined in equation (7). Since, for a given wavelength and the detector distance, Q_{min} is proportional to the beam size at the detector, measurement conditions were chosen to give the same ideal beam size at the detector : pinhole collimation with $A_{1P} = 0.95$ cm and $A_{2P} = 0.48$ cm, and a focusing lens configuration with 28 MgF$_2$ lenses, $A_{1L} = 1.91$ cm, and $A_{2L} = 1.43$ cm. In both cases the ideal beam size at the

Figure 4
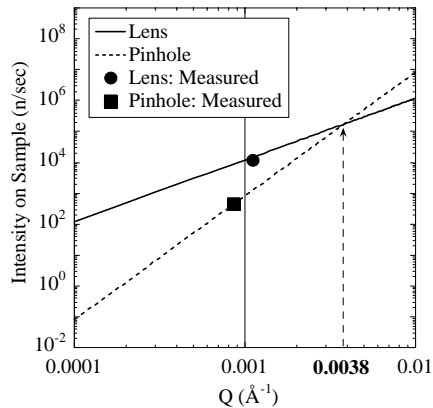Beam profiles measured with a He^3 2D detector. For both the lens and pinhole configuration, $\lambda = 8.44$ Å, $\Delta\lambda/\lambda = 11\%$ and $L_1 = L_2 = 15.7$ m. $A_{1P} = 0.95$ cm, $A_{2P} = 0.48$ cm, $A_{1L} = 1.91$ cm, and $A_{2L} = 1.43$ cm. 28 MgF$_2$ lenses were used for the lens configuration. The total intensity ratio, I_L/I_P, is 26. The smearing factors are $c_P = 1.91$ and $c_L = 2.45$ at SNR $= 10^{4.3}$.

detector is 1.91 cm. Here it should be noticed that $A_{1L} = 2\,A_{1P}$ and $A_{2L} = 3\,A_{2P}$. All other conditions were kept same in both cases, $\lambda = 8.44$ Å, $\Delta\lambda/\lambda = 11\%$ and $L_1 = L_2 = 15.7$ m.

In this case, the beam intensity profiles were measured with the SANS instrument's He^3 2D detector (spatial resolution ~ 0.5 cm). The measurements were made in two steps due to the limited dynamic range of this detector. First, the central regions of the profiles were measured with a plexiglass beam attenuator (with a known attenuation factor) placed right before the source aperture. Second, the wings of the profiles were measured with the attenutator removed and a 2.54 cm beamstop placed at the center of the detector. The central (rescaled with the attenutation factor) and wing profiles were joined to give the full intensity profiles.

Figure 4 shows the intensity profiles for the lens and the pinhole measurements. In both cases, the signal to noise ratio is about $10^{4.3}$ at the points indicated by the arrows in the figure. The total intensity gain of the lens configuration compared with the pinhole collimation is 26, which is nearly equal to the product of the squares of the ratios of aperture diameters multiplied by the neutron transmission of the lenses ($T_L = 0.72$). To make a fair comparison, however, we need to consider the actual beam sizes. The lens collimation results in a slightly larger beam than the pinhole collimation, which can be

quantified in terms of the smearing factors, $c_P = 1.91$ and $c_L = 2.45$ at the signal-to-noise ratio of $10^{4.3}$. Using equations (2) and (5), $Q_{min} = 0.00086$ Å^{-1} for the pinhole configuration and $Q_{min} = 0.0011$ Å^{-1} for the lens configuration. If we consider the smearing factors and Q_{min}, the actual gain of the lens configuration is less than 26.

Figure 5
Estimated intensity gain as a function of Q_{min}. The measured smearing factors, $c_P = 1.91$ and $c_L = 2.45$ for SNR $= 10^{4.3}$, were used. $\lambda = 8.44$ Å, $\Delta\lambda/\lambda = 11\%$, $L_1 = L_2 = 15.7$ m, $A_{1P} = 2 A_{2P}$, and $A_{2L} = 1.59$ cm. The crossover point is $Q_{min} = 0.0038$ Å^{-1}.
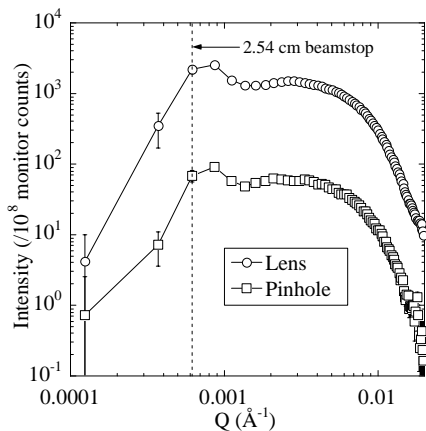
Figure 6
Comparison of the scattering intensities from an aluminium sample. For both the lens and pinhole configurations, $\lambda = 8.44$ Å, $\Delta\lambda/\lambda = 11\%$ and $L_1 = L_2 = 15.7$ m. $A_{1P} = 0.95$ cm, $A_{2P} = 0.48$ cm, $A_{1L} = 1.91$ cm, and $A_{2L} = 1.43$ cm. 28 MgF$_2$ lenses were used. The scattering intensity for the lens configuration is about 25 times higher than for the pinhole configuration. The first valid data point is $Q = 0.0011$ Å^{-1}.

To make a direct comparison, the intensities on sample for both the lens and pinhole configurations were calculated as a function of Q_{min}, shown in figure 5. In these calculations, equations (4) and (6) were used with $\lambda = 8.44$ Å, $\Delta\lambda/\lambda = 11\%$, $L_1 = L_2 = 15.7$ m and the measured smearing factors $c_P = 1.91$ and $c_L = 2.45$. For the lens configuration with 28 MgF$_2$ lenses, $A_{2L} = 1.59$ cm and $T_L = 0.72$ were used. In this case, the crossover Q_{min} is 0.0038 Å^{-1} and the gain of the lens configuration at $Q_{min} \sim 0.001$ Å^{-1} is greater than 1 order of magnitude. The solid circle shows the measured value, derived from

figure 4, for the lens configuration and the solid square for the pinhole configuration.

Figure 6 shows scattering patterns from a single crystal of aluminium containing voids (denoted AL-7 and kindly provided by G. Wignall, Oak Ridge Naltional Laboratory, Hendricks et al., 1974) measured with the lens and pinhole configurations. The sizes of apertures, L_1, L_2, and the number of lenses were the same as used in the beam profile measurements shown in figure 4. To block the direct beam to the detector, a 2.54 cm beamstop was used. In both cases, the counting time was 30 minutes. The measured intensities were normalized with a neutron monitor counts (10^8 counts) and corrected for background, and empty cell scattering. In this case, the scattering intensity for the lens configuration is about 25 times higher than for the pinhole configuration. Considering the beam profiles shown in figure 4 and the beamstop size, the first data point, unaffected by the beamstop occurs at $Q = 0.0011$ Å^{-1}. For the pinhole configuration, the aperture sizes could be slightly relaxed to increase the beam intensity while maintaining the same Q_{min}, but the intensity gain provided by the lenses would still be greater than 10.

4. Conclusion

The focusing properties of multiple biconcave MgF$_2$ lenses have been shown to extend the lower limit of Q in long flight-path small angle neutron scattering instruments. The signal-to-noise ratio of cold neutrons focused by 28 MgF$_2$ lenses is greater than 10^4, the small angle scattering from the lenses is negligible and the beam attenuation by the lenses is manageable. The focusing lens configuration outperforms conventional pinhole collimation at, for the NIST 30m SANS instruments, Q_{min} below ~ 0.004 Å^{-1}. Compared with pinhole collimation, the intensity gain of the lens configuration at Q_{min} around 0.001 Å^{-1} is greater than 1 order of magnitude. This gain extends the lower limit of the accessible Q and would make many previously impractical SANS measurements possible.

References

Alefeld, B., Hayes, C., Mezei, F., Richter, D. & Springer, T. (1997). *Physica B*, **234-236**, 1052-1054.
Barker, J.G. & Glinka, C.J. (1993). *SPIE Proc.* **1738**, 386-394.
Born, M. & Wolf, E. (1975). *Principles of Optics*, Pergamon Oxford.
Eskildsen, M.R., Gammel, P.L., Isaacs, E.D., Detlefs, C., Mortensen K., and Bishop, D.J. (1998). *Nature*, **391**, 563-566.
Glinka, C.J., Barker, J.G., Hammouda, B., Krueger, S., Moyer, J.J. & Orts W.J. (1998). *J. Appl. Cryst.* **31**, 430-445.
Hendricks, R.W., Schelten, J., & Schmatz, W. (1974). *Phil. Mag.* **30**, 819-837.
Lartigue, C., Copley, J.R.D., Mezei, F. & Springer, T. (1995). *J. Neut. Res.* 5, 71-79.
Maier-Leibnitz, H. & Springer, T. (1963). *React. Sci. Technol.* 17, 217-225.
Mildner, D.F.R. & Carpenter, J.M. (1984). *J. Appl. Cryst.* 17, 249-256.
Sears, V.F. (1989) *Neutron Optics*, Oxford University Press.